ELSEVIER

Physica E 9 (2001) 60–68

PHYSICA E

www.elsevier.nl/locate/physe

Thermal conductance through discrete quantum channels

K. Schwab, J.L. Arlett, J.M. Worlock [1], M.L. Roukes *

Condensed Matter Physics, California Institute of Technology, Caltech 114-36, Pasadena, CA 91125, USA

Abstract

We have observed a quantized limiting value of the thermal conductance for each propagating phonon channel in a one-dimensional (1D), ballistic phonon waveguide: $g_0 = \pi^2 k_B^2 T/3h$. To achieve this we have developed nanostructures with full three-dimensional relief that incorporate integral thermometers and heaters. These devices are comprised of an isolated thermal reservoir (phonon cavity) suspended above the sample substrate by four narrow insulating beams (phonon waveguides) with lateral dimensions ~ 100 nm. We employ DC SQUID noise thermometry to measure the temperature of the phonon cavity non-perturbatively. Direct electrical contact from the suspended nanostructure to the room-temperature environment, crucial for these experiments, is attained by means of a very significant level of electrical filtering. These first experiments provide access to the mesoscopic regime for phonons, and open intriguing future possibilities for exploring thermal transport in very small systems. We are currently adapting and improving the ultrasensitive, extremely low dissipation DC SQUID techniques utilized in this work toward the ultimate goal of detecting individual thermal phonons.

PACS: 05.60.Gg; 63.22.+m; 66.70.+f; 85.30.Vw

Keywords: Quantized thermal conductance; Phonons; Nanostructures; Mesoscopics

1. Introduction and motivation

In this paper we describe an experimental system that clearly demonstrates mesoscopic phonon physics in one dimension. Reduced dimensional phonon transport has received theoretical attention from a number of researchers [1–5]. Their efforts have led to the prediction of a *universal quantum of thermal conductance*: $g_0 = \pi^2 k_B^2 T/3h$. This value of thermal conductance exists for each propagating, ballistic, one-dimensional (1D) channel that connects two thermal reservoirs. The thermal conductance quantum is analogous to the quantum of electronic conductance observed in ballistic electron systems [6,7], and is explained with a very similar theoretical description [8].

The theoretical starting point is the Landauer picture for ballistic electron transport. We write the heat current carried between two thermal reservoirs of phonons as

$$\dot{Q} = \sum_{\alpha} \int_0^{\infty} \mathrm{d}k \omega_{\alpha}(k) v_{\alpha}(k) (\eta_{\mathrm{hot}} - \eta_{\mathrm{cold}}) T_{\alpha}(k), \qquad (1)$$

* Corresponding author. Tel.: +1-626-395-2287; fax: +1-626-683-9060.

E-mail address: roukes@caltech.edu (M.L. Roukes).

[1] Permanent address: Department of Physics, University of Utah, Salt Lake City, UT, USA.

1386-9477/01/$ - see front matter
PII: S1386-9477(00)00178-8

where $\omega_\alpha(k)$ is the dispersion relation for phonon branch α, $v_\alpha(k)$ is the group velocity, $\eta = (\exp(\eta\omega/k_B T) - 1)^{-1}$ are Bose–Einstein occupation factors for the two (hot/cold) thermal reservoirs, and $T_\alpha(k)$ are transmission coefficients characterizing the coupling of the propagating waveguide modes between these reservoirs. As with the electron case, when we move from integrating over wave vector k, to frequency ω, the group velocity cancels the 1D density of states. In this case, the thermal conductance depends solely upon the mode thresholds [4].

Eq. (1) simplifies with two assumptions. Firstly, we assume that the transmission coefficients can be engineered so that $T_\alpha(k) = 1$ over some appreciable range of parameters accessible to experiment. As we will show with our measurements, this can indeed be achieved in practice. Secondly, we assume that the temperature is low enough so that only the massless branches of the phonon dispersion relation make significant contribute to the thermal conductance. (By massless branches, we mean those where $\omega_\alpha(k = 0) = 0$.) This condition will be satisfied, roughly, when the thermal phonon wavelength exceeds the waveguide width: $\lambda_{th} = hc/k_B T > w$, where h is Planck's constant, c is the speed of sound, k_B is the Boltzman constant, T is the temperature, and w is the waveguide width. In this limit, it is found that the thermal conductance of a ballistic, 1D channel is limited by the maximum value

$$g_0 = \frac{\pi^2 k_B^2 T}{3h}. \tag{2}$$

For these special modes, the quantized conductance depends solely upon absolute temperature and fundamental constants.

Similar to the case of the quantum of electrical conductance, e^2/h, observed in ballistic electronic systems, the quantization of g_0 is not expected to be manifested with the precision exhibited by quantized angular momentum in atoms, quantized circulation in superfluids, or quantized magnetic flux in superconductors. In these systems the quantization is perfect because it is a consequence of quantum interference of the wavefunction around a closed path. For the "transport quanta", the precision of quantization is instead limited by the engineering and quality of transmission coefficients [9]. [2]

Furthermore, unlike the case for quantization of electrical conductance, we do not expect to observe steps as the phonon thermal wavelength is varied with temperature. In the electronic case at low temperatures, thermal smearing is small for $E_F \gg k_B T$, and transport is, in essence, dominated by electrons of a single wave vector, k_{Fermi}. Steps in electrical conductance arise from the discrete nature of the quantized transverse states that allow electrons to propagate through the constriction. As the constriction width is varied by electrostatic gates, these levels are sequentially populated or depopulated; these events can be individually resolved at low temperatures since the distribution function can be sharp compared to the level spacing. This is not the case with phonons; loosely speaking, the width of the Bose energy distribution is comparable to the average energy and does not allow resolution of individual levels beyond those that are the lowest-lying. Hence, in this case, only one "step" is expected in the conductance at low temperatures, approximately below $\lambda_{therm} = hc/k_B T > w$ [4]. In addition, because of the additional wave polarizations and different boundary conditions, the final number of channels for the phonon case remains $N = 4$ as we scale the waveguides width progressively downward. For the electronic case, by contrast, the number of channels goes to zero as the channel is pinched off.

A very interesting observation is that this result for the thermal conductance is independent of particle statistics [1,10–12]. For this reason the quantum of thermal conductance is truly universal, independent not only of material characteristics but also of the quantum statistics of the particles that transport the energy. In addition, there exists a deep connection to quantum limits of information flow [1,13,14]. The quantum of thermal conductance is the maximum thermal conductance per channel and this is equivalent to the maximum data rate down a 1D channel. This appears to have been first pointed out by Pendry [1], who considered the connection between maximal

[2] An interesting exception is the quantum hall effect where the quantization of the hall resistance is precise in multiples of e^2/h and is *not* a result of interference. In this ballistic system, the transmission coefficients are nearly perfect because of the macroscopic spatial separation between the channels with $+k$ and $-k$ which suppresses any back scattering mechanism.

information flow, maximal entropy flow, and maximal heat flow. By following this chain of reasoning, he concluded that the maximum thermal transport through a 1D channel, for either Fermi or Bose statistics, is given by the quantum of thermal conductance.

The dispersion relations for the vibrational modes of a dielectric beam of square cross-section have been calculated using numerical techniques [15]. Although the spectra of the massive modes are very complex, one finds that there exists four massless branches: one longitudinal (dilatational), one torsional, and two transverse branches. Thus, for a freely suspended, dielectric beam at low temperatures, we expect to observe a maximum thermal conductance of $4g_0$.

The transmission coefficients for longitudinal waves have been calculated [3] for different waveguide shapes. A catenoidal shape, $\cosh^2(x/\lambda)$, has superior transmission coefficients, closer to unity over a wider range of energies, compared to those for a linear taper. These calculations also show that as one lowers temperature, thereby increasing the phonon wavelength, the transmission coefficients eventually fall to zero. This "loss of adiabaticity" arises from the finite size of the waveguide termination, W. For very long wavelength (i.e. at the sufficiently low temperatures), $\lambda_{\text{therm}} > W$ and the reservoir/waveguide junction will appear as a discontinuity in the acoustic impedance, and result in the reflection of incident power. Because of this we expect to observe the quantized value for the thermal conductance only over a finite-temperature range, where $W > \lambda_{\text{therm}}(T) > w$ (w is the waveguide width, and W is the waveguide termination width).

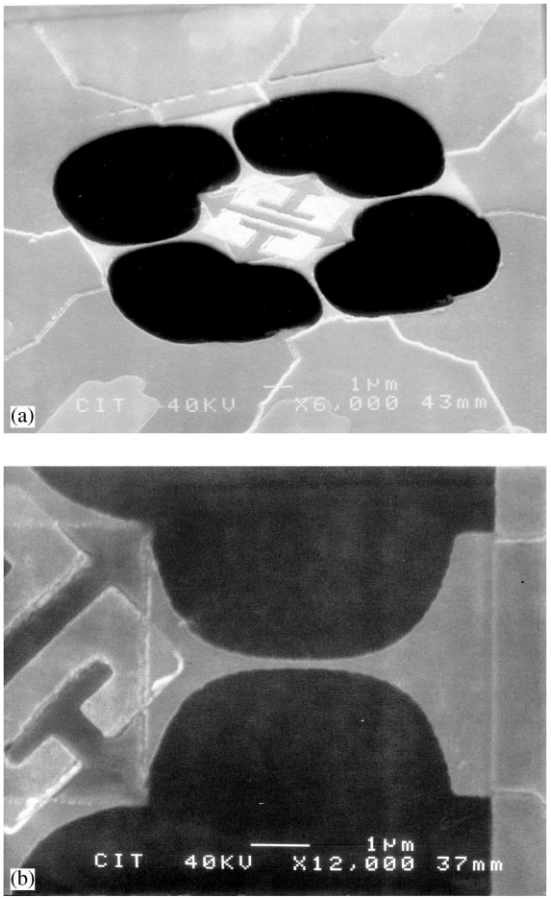

Fig. 1. Suspended mesoscopic phonon device. (a) View of the suspended device, which is comprised of a 4×4 μm "phonon cavity" (center) patterned from a 60 nm thick silicon nitride membrane. The bright "C" shaped objects on the cavity are thin film Cr/Au resistors, whereas in the dark regions the membrane has been completely removed. The resistors are connected to thin film Nb leads that run atop the "phonon waveguides"; these leads ultimately terminate at the wirebond pads. (b) Close up of one of the freely suspended catenoidal waveguides, displaying the narrowest region which necks down to < 200 nm width.

2. Experiment

2.1. Nanofabricated sample

Fig. 1 shows a typical nanofabricated device [16]. The essential elements of the sample are its central silicon nitride "plate", the phonon cavity, which is suspended from the substrate by four narrow beams of rectangular cross section, the phonon waveguides. On the phonon cavity we have deposited two Cr/Au resistors (of thickness 5/25 nm), one to serve as a heater and the other as a thermometer. On top of the phonon waveguides we deposit 25 nm of Nb to provide superconducting leads to the Cr/Au resistors.

This sample has been engineered to satisfy four conditions that are necessary to realize the thermal conductance quantum with phonons:

(a) Isolated phonon thermal conductance: We use superconducting Nb films on top the phonon waveguides to contact the Cr/Au resistors. This eliminates the parasitic electronic thermal con-

duction that has obfuscated previous experiments [17].

(b) One-dimensional limit: The minimum cross section of the phonon waveguides is 200 nm × 85 nm. The phonon thermal wavelength in silicon nitride is $\lambda_{\mathrm{therm}} = 300\,\mathrm{nm}/T$, where T is the temperature in kelvin. Thus, for temperatures $T < 1.5$ K, we begin to enter the 1D limit.

(c) Adiabatic contacts: We have drawn our sample to the shape $\cosh^2(x/\lambda)$. The transmission coefficients for longitudinal sound through a waveguide of this shape has been calculated [3] and are found to provide superior (nearly adiabatic) coupling as compared to a linearly tapered horn. However, because these waveguide terminations are finite, we still expect loss of adiabaticity at temperatures where the phonon wavelength exceeds 4 μm. From the calculations in Ref. [3], we expect this to occur for $T < 10$ mK in these devices.

(d) Ballistic transport: Ideally, one would utilize crystalline materials to achieve ballistic transport of phonons [18]. However, because of fabrication difficulties we used free standing, 60 nm thick, silicon-rich, low-stress silicon nitride films in these first experiments. Two groups have measured the thermal conductance of low-stress silicon nitride films [19,20]. It is found that for temperatures $T > 1$ K, the phonon mean free path is limited by diffuse boundary scattering, the Casimir limit. However, as the temperature is lowered, the mean free path increases and the transport becomes predominantly ballistic. At first impression it may seem surprising that ballistic transport can be achieved within an apparently glassy, non-stoichiometric material. This can be understood by noting that as phonon thermal wavelength grows the material appears to be increasingly homogeneous, thus providing a smooth effective medium for the acoustic wave.

To measure the thermal conductance we need to be able to force a heat current, $\dot{Q}$, to flow in the phonon waveguides and measure the resulting temperature drop, ΔT, along them. For small ΔT, the thermal conductance is given by $G = \dot{Q}/\Delta T$. However, because of the experimental conditions, especially temperature regime and size scale, providing heat to the sample and measuring temperature both prove to be quite challenging.

2.2. Thermometry

Thermometry is a significant problem on the microscopic sample employed in this study. The measurement power is severely restricted by the exceedingly weak coupling between the electron gas and the lattice at low temperatures [21]. As an estimate of the maximum power, $\dot{Q}$, which can be dissipated into the electron gas we use the measured electron–phonon coupling:

$$\dot{Q} = \Omega\Sigma(T_{\mathrm{e}}^5 - T_{\mathrm{p}}^5), \tag{3}$$

where Ω is the volume of the electron gas, $\Sigma = 2 \times 10^9\,\mathrm{W/m^3K^5}$ is the electron–phonon coupling strength, T_{e} is the temperature of the electron gas and T_{p} is the lattice temperature. For our sample with $\Omega = 0.1\ \mu\mathrm{m}^3$, the electrons will remain at $T_{\mathrm{e}} = 50$ mK with the lattice at $T_{\mathrm{p}} = 0$ K with only $\dot{Q} = 10^{-16}$ W of power dissipated into the electron gas.

To overcome this problem we are utilizing DC SQUID-based noise thermometry [22–24]. In this technique, the temperature of a resistor is measured by placing it in a superconducting circuit that tightly couples it to a SQUID which amplifies the Nyquist current noise generated by the resistor. By the Fluctuation–Dissipation theorem (see, example Ref. [25]), we know that current fluctuations are driven in the SQUID input circuit by the dissipative elements, namely, by the thermometer resistor. Fig. 2 shows our measurement circuit; the SQUID-based noise thermometry is on the right-hand side of the diagram. We use a superconducting transformer T1 ($L_{\mathrm{p}} = 2.3\,\mathrm{mH}, L_{\mathrm{s}} = 1.6\ \mu\mathrm{H},\ k = 0.78$) to amplify the current noise and to place all of the Nyquist noise-current spectral density into a low-frequency band. We use a second DC SQUID (SQ2) as a ultralow noise preamp ($\sim 20\,\mathrm{pV}/\sqrt{\mathrm{Hz}}$) to read out the front-end DC SQUID (SQ1). This is necessary to avoid degrading the ultralow noise floor of SQ1.

At first glance it appears that there will be no power dissipated within the thermometer resistor with our measurement scheme. There are, however, at least two sources of dissipation into the measured resistor that can be identified: Josephson radiation from the SQUIDs, and current fluctuations from the resistive shunts at the SQUIDs Josephson junctions. The Josephson radiation arises from the fact that the SQUIDs are always operated in the finite-voltage state;

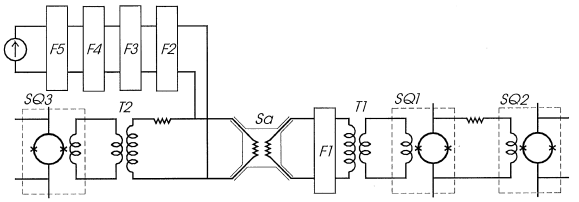

Fig. 2. Measurement schematic. The suspended sample (Sa), cooled on the dilution refrigerator's mixing chamber (MXC), is represented by two ($\sim 17\ \Omega$) resistors in the center of the figure. Its rightmost (sensor) transducer is coupled to a DC SQUID-based noise thermometry circuit. Two thin-film DC SQUIDs (SQ1, SQ2) are cooled on the MXC to enable ultralow-noise performance: SQ1 is run open loop (with continuous gain measurement carried out at 900 Hz, i.e. just outside the noise measurement band) while its readout, SQ2, is operated in flux-locked mode. The metallic powder filter (F1) on the MXC, shields the sample from Josephson radiation emanating from the SQUIDs. The sample's leftmost (heater) resistor is connected to a heavily filtered (F2–F5) current biasing circuit used to Joule heat the nanostructure. A SQUID voltmeter circuit (SQ3) on the MXC allows resistance measurement in situ, by sensing the voltage drop across the current-biased heater. The heavily shielded superconducting transformers (T1, T2) provide a current gain of ~ 18. The cold sample is isolated from heat conduction from the higher-temperature environment through filters F2 and F3 (cooled on the MXC) and F4 and F5 (at 700 mK). F2 and F4 are metallic powder filters, while F3 and F5 are 10 pole RC filters.

there is an oscillatory circulating current within the SQUID loop. These oscillations occur at the Josephson frequency for the bias point chosen, and are typically about 10 GHz for our SQUIDs. This narrow-band, high-frequency radiation can be attenuated without affecting the low-frequency measurement band. Fig. 2 shows the placement of a lossy stainless-steel powder filter, F1, which is used to absorb this radiation. Because of the weak coupling between the electrons and the lattice at low temperatures, it is likely that the SQUIDs shunt resistors will not cool below ~ 200 mK, even for colder dilution refrigerator mixing chamber temperatures [26]. Hence, we estimate that the total available power which can flow from the SQUID shunts to the Cr/Au noise thermometer resistor to be $\sim 10^{-20}$ W. In this estimate we have limited the bandwidth of the noise power radiating from the SQUID to ~ 1 MHz, which is reasonable given the known frequency response of our coupling transformers.

2.3. Heater circuit

In order to supply Joule heat to the nanostructure, we need a DC connection from room-temperature electronics to the Cr/Au heater resistor on the phonon cavity held at low temperature. However, the thermal radiation from resistors at higher temperatures (in the form of Johnson noise) is a significant problem. One can show that the total available power that can be transferred from a resistor at temperature T to one at 0 K is

$$\dot{Q} \approx \frac{k_B^2 T^2}{h}. \tag{4}$$

The frequency of this Johnson noise power will extend from DC to ν_{max}, where $h\nu_{max} \sim k_B T$. For example, a resistor at 1 K has a total available power of 0.3 pW and spectrum extending to 40 GHz. This power would prevent our sample from cooling below 1 K. Because of this, the connection from the suspended nanostructure to the thermal environment must be carefully engineered.

In order to circumvent this problem we have installed an extensive filter network between the sample on the mixing chamber and the room-temperature electronics. We have installed two sets of filters, one set (F4 and F5) on the "still", i.e. typically at ~ 0.7 K, and another set (F2 and F3) at the (coldest) sample stage on the mixing chamber of the dilution refrigerator. The filters at 0.7 K adsorb the radiation from 300 K, while the set at the sample temperature adsorb the power radiated at 0.7 K by the dissipative elements of the filters. Each filter set consists of a 10 pole RC filter (F3 and F5) made from microwave components, and a stainless-steel powder filter (F2 and F4). The RC network is effective from 1 kHz to ~ 1 GHz, while the lossy powder filter [27] provides significant attenuation from 100 MHz to > 20 GHz (the latter being limit of our network analyzer) Fig. 3 shows the total filter attenuation, which is the sum of the measured performance of each filter element, F2–F5. We believe that we have limited the total power radiated to the sample from 300 K to be less than 10^{-18} W, and less than 10^{-19} W from 0.7 K. In addition to the filters, the sample is isolated inside a close-fitting superconducting Pb cavity. Only two twisted pairs penetrate this cavity, one pair for the thermometer and the other for the heater. These twisted pairs, which

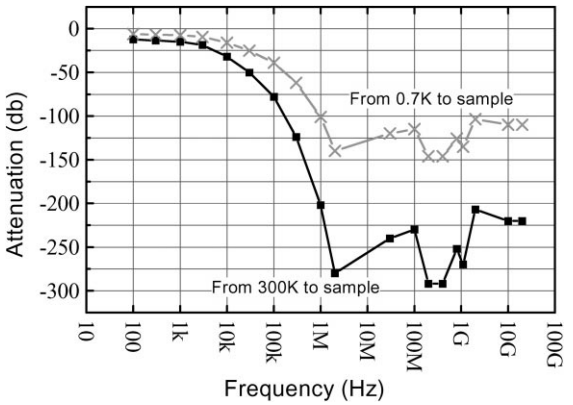

Fig. 3. Filter performance. We use a cryogenic filter network to isolate the sample from the external thermal environment, which is connected through the heater leads. Data with crosses shows attenuation between the sample and the filters set at 0.7 K, while the data with squares shows the attenuation between the sample and room-temperature environment at 300 K.

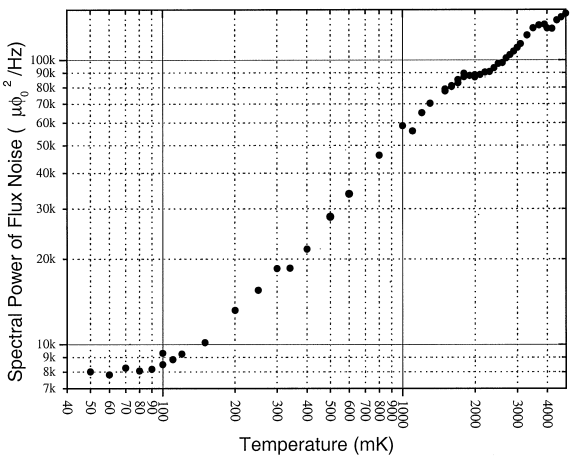

Fig. 4. Noise thermometer. The measured spectral noise power of the SQUID flux noise is plotted vs. refrigerator temperature. For temperatures 80 mK $\leqslant T \leqslant$ 1.8 K, the behavior closely follows the form of ideal Nyquist current noise.

are themselves shielded in superconducting Nb capillary, connect the sample with the transformer coupled SQUID electronics.

Fig. 2 shows the heater side of the circuit. In addition to the filter network, we have installed a DC SQUID voltmeter at the sample temperature with an input impedance of 10 kΩ and a sensitivity of $\sim 1 \times 10^{-9}$ V/$\sqrt{\text{Hz}}$. We use this to measure the voltage developed across the device while we apply the heater current. Together with the calibrated source of applied current at room-temperature, these elements provide an accurate measure of the Joule heat deposited into the phonon cavity.

2.4. Additional details

These nanostructures have proven to be extremely sensitive and susceptible to electronic shock. In order to make wirebonds to the sample, we fabricate a large, 200 nm thick, Au shorting resistor across the bond pads which lead to the Cr/Au resistor on the nanostructure. After wirebonding, we use a scribe to open this shorting resistor. In order to make the connections to the measurement electronics without damaging the sample, we epoxy the 3 mm $\times$ 3 mm silicon substrate, which supports the nanostructure, onto a 2.5 cm $\times$ 2.5 cm glass slide. On this slide we deposit a 50/10 nm thick Nb/Au meander. This 9 kΩ meander makes contact from the bond pads leading to each side of the Cr/Au resistor on the nanostructure, to a large pad where we make contact to the measurement electronics with pressed In contacts. This short between the two sides of the meander, $\sim$ 100 Ω, is then mechanically removed with a scribe when the contact to the measurement electronics is complete. At room temperature this meander provides both a resistive divider (100 Ω/9 kΩ) and a series resistance of 9 kΩ that protects the sample. However, at low temperatures the meander superconducts and thus becomes transparent to the measurement electronics. Without these measures we have found that the nanostructure melts at the cantenoid when contacted electronically, presumably from heat deposited by electronic shock.

3. Experimental results

Fig. 4 shows the measured noise thermometry data. We first stabilize the dilution refrigerator at a target temperature, and then measure the amplitude of the noise generated by the thermometer resistor as detected by the DC SQUID noise thermometer. The noise power is integrated within a band 500 Hz wide, centered at 1250 Hz, for 200 s. In Fig. 4, we plot the

spectral density of the flux noise vs. the temperature of the dilution refrigerator as measured by a calibrated Ge resistance thermometer. For temperatures in the range 80 mK–1.8 K, we find that the spectral density of the flux noise scales linearly with temperature, as expected from the Nyquist noise formula. For temperatures greater than 1.8 K, the noise deviates from linear behavior, which is probably caused by the loss of superconductivity of the film on top the phonon waveguide. For temperatures less than 80 mK, the noise power saturates. This may be caused by an unknown source of power, of magnitude $\sim 10^{-16}$ W, which is coupled into the Cr/Au resistor thereby elevating its electron temperature above that of the lattice [21]. The slope of the noise power in the temperature range 80 mK–1.8 K is consistent with a noise thermometer resistance of 9 Ω. This value is close to the measured value of its nominally identical twin, the resistor used as the heater, $R_{\text{heater}} = 17\ \Omega$. Without the noise thermometer circuit connected to the input coil of the SQUID SQ1, we typically achieve a noise floor about $\sim 1\mu\phi_0/\text{rt Hz}$, which is a coupled energy sensitivity of 3.3×10^{-32} J/Hz = 50 h. Using this resistance and energy sensitivity of our SQUID system, we expect a noise temperature of our SQUID system [22] to be 500 μK.[3] However, the intercept of the fit line gives the measure of the SQUID system noise of 50 mK. This excess noise cannot be attributed to our measurement circuit and may reflect mesoscopic phenomena within the Cr/Au resistor. It is interesting to speculate that there may be some connection between the observed saturation in the noise temperature and the excess noise power.

The thermal conductance is measured by first stabilizing the dilution refrigerator at the desired temperature and then measuring the noise temperature for different steady-state power levels deposited into the heater. At each temperature, we measure the heater resistance. In this way we obtain an accurate measurement of Joule power, $\dot{Q}$, deposited into the nanostructure. Fig. 5 shows the measured noise thermometer response vs. heater power taken at 450 mK. The scatter in the points is consistent with the expected statistical uncertainty [28] given our measurement bandwidth,

[3] The noise temperature is defined as the temperature at which the noise generated by the resistor will equal the noise of the SQUID system.

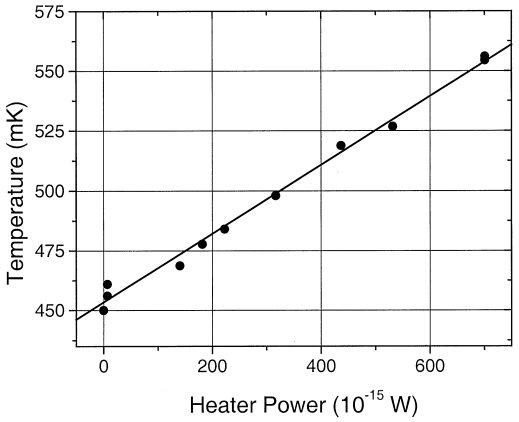

Fig. 5. Noise temperature vs. heater power. The measured noise temperature of the Cr/Au thermometer resistor is plotted vs. the power delivered to the Cr/Au heater resistor, measured at 450 mK. The inverse of the slope of the fit line gives the thermal conductance of the nanostructure.

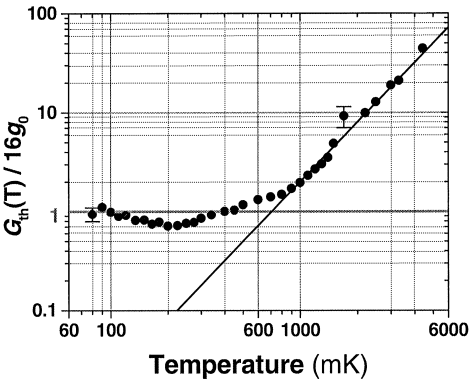

Fig. 6. Thermal conductance. The measured thermal conductance versus temperature is displayed. For temperatures $T > 0.8$ K we observe T^3 behavior, which is consistent with a mean free path of ~ 1 μm. For temperatures $T < 0.8$ K we observe a transition to linear behavior with a value approaching the expected quantum value of $16g_0$.

$\Delta B = 500$ Hz, and integration time, $\tau = 200$ s:

$$\sigma_T \approx T\sqrt{\frac{1}{\Delta B \tau}}. \tag{5}$$

Fig. 6 shows the measured thermal conductance of the phonon waveguides and is the central result of this work. We find for temperatures $T > 0.8$ K that the thermal conductance follows a T^3 law. The data in this regime are consistent with a temperature-independent

mean free path of ~ 1 μm and is within the range observed by other researchers on similar material [19,20]. However, for temperatures below 0.8 K, we see a dramatic transition from the T^3 behavior to what is essentially linear dependence. This is the hallmark of 1D behavior. The transition occurs at a temperature where the thermal phonon wavelength, $\lambda_{\text{therm}} = 380$ nm, is somewhat greater than the width of the phonon waveguide at the constriction. We see that the thermal conductance in this regime is close to the predicted value of $16g_0$ (four massless modes per channel, and four channels). This indicates that we have achieved adiabatic coupling to the waveguide, and ballistic transport.

Because of the saturation in the noise thermometer at ~ 80 mK, we are unable to explore the behavior at lower temperatures where we expect to observe the loss of adiabatic coupling between the phonon waveguide and the reservoirs. We are currently attempting to extend the range of our measurement to these lower temperatures.

The deviations from exact quantization are reminiscent of those observed in electronic systems and could be a result of a number of effects:

(a) *Phonon mean-free path*: Holmes et al. [19] show that the thermal conductance of a 1μm thick, silicon-rich, low-stress silicon nitride sheet approaches the ballistic limit in the temperature range of ~ 200 mK. This could explain the approach to the ideal quantum value of thermal conductance in our data as the sample is cooled below 250 mK.

(b) *Transmission coefficients*: The imperfect quantization could also be caused by non-ideal transmission coefficients, $T_m < 1$. As we decrease temperature and work with phonons of greater wavelength, we are essentially scanning the transmission coefficients vs. wavelength. Since the sample will appear smoother for the longer phonon wavelength, this could explain the approach to the ideal value as we lower the temperature.

(c) *Channel opening effect*: In electronic systems which show quantized electronic conduction, researchers have observed suppression of the conductance at the onset of each channel opening [29]. This is understood [30–32] as a result of enhanced scattering from the open channels into those just at the threshold of opening. However, due to the small longitudinal energy, which can localize the barely open channel, incoming electrons are efficiently backscattered. It has been suggested that a similar effect may be responsible for the dip in the phonon thermal conductance at 250 mK.

4. Conclusions

We have engineered an experiment that allows us to directly observe the contribution to thermal conductance from individual 1D ballistic phonon channels. We have measured a universal limiting value for the thermal conductance per channel $g_0 = \pi^2 k_B^2 T/3h$. We are currently experimenting with additional nanostructures to differentiate between what is truly universal behavior in our observations, and what are mesoscopic, sample-specific effects. This approach has revealed some of the first clear manifestations of mesoscopic phonon physics.

The universal quantum of thermal conductance is of importance for the future engineering of nanoscale devices. In any nanostructure where energy must be dissipated, such as memory or logic elements, g_0 represents the maximum energy transfer rate per thermalization channel. The techniques described in this work are also relevant to researchers interested in extremely low dissipation, non-perturbative measurement – especially those interested in realization of solid-state quantum computing devices [33–35].

The physics demonstrated in this work clearly exhibits the wave-like nature of phonons. In future experiments we hope to explore the particle-like nature through detection of individual quanta [36]. Although technically challenging, this offers the possibility to observe interesting quantum effects such as phonon shot noise and phonon bunching. If successful, such efforts would represent the first detection of a single mechanical quantum, and offers intriguing prospects for producing and detecting novel non-classical phonon states such as squeezed phonon states [37,38].

Acknowledgements

We thank M.C. Cross, R. Lifshitz, G. Kirczenow, and M. Blencowe, N. Wingreen, M. Lilly, and P.

Burke for discussions, suggestions, and insights, and N. Bruckner for assisting in the growth of the low-stress silicon nitride at the University of California, Berkeley Microfabrication Laboratory. We thank M.B. Ketchen and members of the IBM Yorktown superconductivity group for advice, assistance, and the DC SQUID devices employed in our cryogenic electronics. One of us, J.A., would like to acknowledge the support of NSERC. Finally, we gratefully acknowledge the support from DARPA MTO/MEMS and NSF/DMR that enabled this work.

References

[1] J.B. Pendry, J. Phys. A 16 (1983) 2161.
[2] R. Maynard, E. Akkermans, Phys. Rev. B 32 (1985) 5440.
[3] L.G.C. Rego, G. Kirczenow, Phys. Rev. Lett. 81 (1998) 232.
[4] D.E. Angelescu, M.C. Cross, M.L. Roukes, Superlatt. Microst. 23 (1998) 673.
[5] M.P. Blencowe, Phys. Rev. B 59 (1999) 4992.
[6] B.J. van Wees et al., Phys. Rev. Lett. 60 (1988) 848.
[7] D.A. Wharam et al., J. Phys. C 21 (1988) L209.
[8] A. Szafer, A.D. Stone, Phys. Rev. Lett. 62 (1989) 300.
[9] S. Datta, Electronic Transport in Mesoscopic Systems, University Press, Cambridge, 1995.
[10] A. Greiner, L. Reggiani, L. Varani, T. Kuhn, Phys. Rev. Lett. 78 (1997) 1114.
[11] L.C.G. Rego, G. Kirczenow, Phys. Rev. B 59 (1999) 13 080.
[12] I.V. Krive, E.R. Mucciolo, Phys. Rev. B 60 (1999) 1429.
[13] M.P. Blencowe, quant-ph/0001007, Phys. Rev. A, submitted for publication.
[14] C.M. Caves, P.D. Drummond, Rev. Mod. Phys. 66 (1994) 481.
[15] N. Nishiguchi, Y. Ando, M.N. Wybourne, J. Phys.: Condens Matter 9 (1997) 5751.
[16] K. Schwab, E.N. Henriksen, M.L. Roukes, Appl. Phys. Lett., submitted for publication.
[17] T.S. Tighe, J.M. Worlock, M.L. Roukes, Appl. Phys. Lett. 70 (1997) 2687.
[18] T. Klitsner, J.E. VanCleve, J.E. Fischer, R.O. Pohl, Phys. Rev. B 38 (1988) 7576.
[19] W. Holmes, J.M. Gildemeister, P.L. Richards, V. Kotsubo, Appl. Phys. Lett. 72 (1998) 2250.
[20] M.M. Leivo, J.P. Pekola, Appl. Phys. Lett. 72 (1998) 1305.
[21] M.L. Roukes, M.R. Freeman, R.S. Germain, R.C. Richardson, M.B. Ketchen, Phys. Rev. Lett. 55 (1985) 422.
[22] M.L. Roukes, R.S. Germain, M.R. Freeman, R.C. Richardson, Physica B and C 126 (1984) 1177.
[23] M.L. Roukes, Hot Electrons and Energy Transport in Metals at mK Temperatures. Doctoral Dissertation, Deptartment of Physics, Cornell University, 1985.
[24] F. Pobell, Matter and Methods at Low Temperatures, Springer, New York, 1992.
[25] F. Rief, Fundamentals of Statistical and Thermal Physics, McGraw-Hill, New York, 1965.
[26] F.C. Wellstood, C. Urbina, J. Clarke, Phys. Rev. B 49 (1994) 5942.
[27] J.M. Martinis, M.H. Devoret, J. Clarke, Phys. Rev. B 35 (1986) 4682.
[28] R.A. Webb, R.P. Giffard, J.C. Wheatly, JLTP 13 (3/4) (1973) 383.
[29] Y. Hirayama, T. Saku, Y. Horikoshi, Phys. Rev. B 39 (1989) 5535.
[30] A. Yacoby, Y. Imry, Europhys. Lett. 11 (1990) 663.
[31] I. Kander, Y. Imry, U. Sivan, Phys. Rev. B 41 (1990) 12 941.
[32] E. Castano, G. Kirczenow, Phys. Rev. B 45 (1992) 1514.
[33] D. Loss, D.P. DiVincenzo, Phys. Rev. A 57 (1998) 120.
[34] D.V. Averin, Solid State Commun. 105 (1998) 659.
[35] B.E. Kane, Nature 393 (1998) 133.
[36] M.L. Roukes, Physica B 263–264 (1999) 1.
[37] X.D. Hu, F. Nori, Physica B 263–264 (1999) 16.
[38] V. Braginsky, F. Khalili, Quantum Measurement, University Press, Cambridge, 1992.